INORGANIC CHEMISTRY FRONTIERS

RESEARCH ARTICLE

Cite this: *Inorg. Chem. Front.*, 2023, **10**, 6407

A highly connected metal–organic framework with a specific nonpolar nanotrap for inverse ethane/ethylene separation†

Jing-Jing Pang,[a] Zhi-Han Ma,[a] Qiang-Qiang Yang,[a] Kuo Zhang,[a] Xin Lian,[a] Hongliang Huang, *[b] Zhao-Quan Yao,*[c] Baiyan Li, [a] Jian Xu *[a] and Xian-He Bu [a,d]

Received 13th August 2023,
Accepted 13th September 2023

DOI: 10.1039/d3qi01595e

rsc.li/frontiers-inorganic

Efficient separation of ethylene (C_2H_4) from ethane (C_2H_6) *via* a one-step adsorption process is desirable yet challenging. In this work, we report a C_2H_6-selective polynuclear Tb-MOF $[Tb_9(\mu_3\text{-}O)_2(\mu_3\text{-}OH)_{12}(H_2O)_9(TCPE)_3]^-\cdot[H_3O]^+\cdot(solvents)_x$ (TCPE = tetrakis(4-carboxyphenyl)ethylene acid), **NKU-200-Tb**, assembled *via* the reticular chemistry principle. The resulting (4,12)-connected framework critically features a high density of nonpolar aromatic rings on the pore surface and forms a specific nanotrap for C_2H_6 with multiple C–H⋯π interaction sites. As a result, **NKU-200-Tb** exhibits an inverse adsorption behavior with a high C_2H_6/C_2H_4 selectivity of 2.06 and a large uptake ratio of 151% (60.27/39.95 $cm^3\ g^{-1}$) at 298 K and 1 bar. The superior adsorption properties of **NKU-200-Tb**, combined with great structural stability, place it among the most promising stable C_2H_6-selective MOFs. Dynamic breakthrough experiments demonstrate that polymer-grade C_2H_4 (>99.9%) can be harvested in one step from a binary mixture of C_2H_6/C_2H_4 (10/90, v/v). This work signifies the synergy of pore surface chemistry and space confinement in promoting the challenging C_2H_6/C_2H_4 separation.

Ethylene (C_2H_4) is one of the most important chemical feedstocks in the petrochemical industry due to its wide use in the manufacture of polymers, plastics, polyesters, and other commodity chemicals, wherein polymer-grade C_2H_4 (≥99.9% pure) is required.[1] However, the crude olefin products obtained through the cracking of naphtha inevitably contain a small amount of ethane (C_2H_6) impurity, and their separation is presently considered as the most challenging industrial separation ascribed to their very similar molecular dimensions and physicochemical properties (Scheme 1).[2] Cryogenic distillation technology is the prevalent solution in industry for separating C_2H_4 from C_2H_6, which is usually operated in a large distillation tower (120–180 trays) at low temperatures (180–258 K) and high pressures (5–28 bar), thereby coming with a high energy penalty.[3] As far as is known, purification of olefin (*i.e.*, ethylene and propylene) from paraffin (*i.e.*, ethane and propane) accounts for 0.3% of global energy use and has been regarded as one of the "seven chemical separations to change the world".[4] Thus, developing an alternative method of purifying

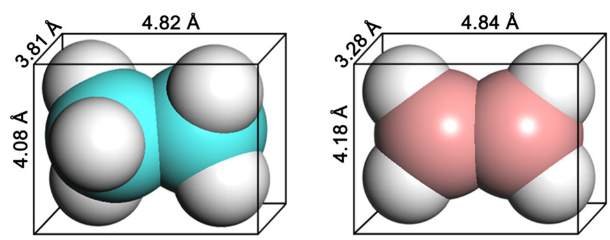

	KD (Å)	BP (K)	Polarizability ($10^{-25}\ cm^3$)	QM (10^{-26} esu cm^2)
C_2H_6	4.4	184.6	44.3	0.65
C_2H_4	4.2	169.5	42.5	1.50

Scheme 1 Molecular structure and physical properties of C_2H_6 and C_2H_4, KD = kinetic diameter. BP = boiling point, QM = quadrupole moment.

[a] *School of Materials Science and Engineering, Smart Sensing Interdisciplinary Science Center, TKL of Metal and Molecule-Based Material Chemistry, Nankai University, Tianjin 300350, China. E-mail: jxu@nankai.edu.cn*
[b] *School of Chemistry and Chemical Engineering, Tiangong University, Tianjin 300387, China. E-mail: huanghongliang@tiangong.edu.cn*
[c] *School of Chemistry and Chemical Engineering, Tianjin University of Technology, Tianjin, 300384, China. E-mail: yaozq@email.tjut.edu.cn*
[d] *State Key Laboratory of Elemento-Organic Chemistry, Frontiers Science Center for New Organic Matter, Collaborative Innovation Center of Chemical Science and Engineering (Tianjin), Nankai University, Tianjin 300071, China*

† Electronic supplementary information (ESI) available: Additional crystallographic and magnetic data. See DOI: **https://doi.org/10.1039/d3qi01595e**

C_2H_4 in an energy-efficient manner is urgently desirable and essential to reduce energy footprint.

Adsorptive separation by porous materials has emerged as a promising technology for addressing olefin purification.[5,6] In this regard, metal–organic frameworks (MOFs) have great advantages over conventional porous solids (*e.g.*, zeolites, activated carbon, and mesoporous silica) in terms of gas adsorption selectivity and capacity, on account of their programmable pore structures and customizable pore environments.[7,8] Over the past decade, many MOF adsorbents have been designedly constructed and shown preferential adsorption of C_2H_4 over C_2H_6, relying on molecular sieving,[9,10] π-complexation,[11] or electrostatic interaction between the π-clouds of olefin and highly polar groups (*e.g.*, open metal sites).[12] In order to obtain polymer-grade ethylene, these C_2H_4-selective adsorbents have to be subjected to multiple adsorption–desorption cycles to remove the co-adsorbed impurity, inevitably involving energy-intensive desorption and regeneration steps by temperature or vacuum swing.[13] In contrast, the adsorbents with inverse adsorption selectivity for C_2H_6 over C_2H_4 can harvest pure C_2H_4 directly at the outlet through a single-step adsorption process with about 40% energy saving.[14–17] However, such C_2H_6-selective adsorbents reported to date are much fewer than the C_2H_4-selective ones probably due to two major reasons: first, the kinetically driven separation or molecular sieving is inaccessible for achieving inverse adsorption behavior in rigid MOFs, as the kinetic diameter of C_2H_6 is larger than that of C_2H_4. Second, there is a lack of suitable strong paraffin affinity sites compared with olefin, bringing difficulty in designing delicate pore environments to trap C_2H_6.

In recent five years, significant efforts have been dedicated to the construction of non-trivial paraffin-selective MOFs and gained much progress.[18] Among the proposed design strategies, the most sophisticated one is to customize an inert/hydrophobic pore surface composed of nonpolar aromatic rings or aliphatic chains in the absence of open metal sites, which is envisaged to attain more nonspecific van de Waals (vdW) interactions with C_2H_6 due to its larger polarizability than C_2H_4 (44.3×10^{-25} cm^3 *vs.* 42.5×10^{-25} cm^3) and more C–H binding sites.[19] With this principle, a series of C_2H_6-selective MOFs have been successfully fabricated,[20–23] but many of them suffer from insufficient C_2H_6/C_2H_4 selectivity (<2) partly due to the relatively weak interaction nature of vdW forces. One straightforward way to overcome this dilemma is increasing the number of such vdW interactions by promoting the density of functional affinity sites or enhancing confinement to enlarge the contact area of the pore surface with gas molecules, both of which are, however, still underexplored. In addition to adsorption properties, the structural stability of adsorbents should also be considered. For example, $Fe_2(O_2)$(dobdc) with a record C_2H_6/C_2H_4 selectivity has to be operated in a glove box because of its poor stability in environments,[15] greatly hindering its industrial application.

Bearing these in mind, we sought to explore the adsorption and separation performance of a (4,12)-connected Tb-MOF, namely **NKU-200-Tb**,[24] based on a nonanuclear Tb_9 node and the aromatic linker tetrakis(4-carboxyphenyl)ethylene acid (H_4TCPE, Fig. S1 and S2†), due to the following considerations. First, its highly connected **shp** network constitutes a large π-conjugated system enriched with nonpolar aromatic rings, promoting the density of functional affinity sites for C_2H_6. Second, its framework contains three types of channels with different shapes and apertures, holding high promise to offer suitable confinement and multi-site adsorption for C_2H_6. Third, the high connectivity of the framework and the strong coordination bond between the Tb^{3+} ion (hard Lewis acid) and carboxylate ligand (hard Lewis base) endow it with excellent structural stability. In line with the above analyses, **NKU-200-Tb** shows the desired inverse adsorption behavior with a high C_2H_6/C_2H_4 selectivity of 2.06 at 298 K and 1 bar, surpassing many reported C_2H_6-selective MOFs. Further density functional theory (DFT) calculations disclose that the aperture window of one channel with suitable pore size forms a nanotrap to promote the C_2H_6/C_2H_4 separation by the enhanced confinement. As a result, **NKU-200-Tb** achieves a good performance for purifying C_2H_4 (>99.9%) in one step from a binary mixture of C_2H_6/C_2H_4 (10/90, v/v), as demonstrated by breakthrough experiments, placing it among the promising one-step C_2H_4 purification adsorbents.

The crystalline **NKU-200-Tb** was synthesized according to our previous report.[24] Single-crystal X-ray diffraction analysis reveals that it crystallizes in the trigonal space group $P\bar{3}$ with the formula $[Tb_9(\mu_3\text{-}O)_2(\mu_3\text{-}OH)_{12}(H_2O)_9(TCPE)_3]^-\cdot[H_3O]^+\cdot(\text{solvents})_x$ (Fig. S3 and Table S1†). In this structure, the nonanuclear carboxylate-based cluster $[Tb_9(\mu_3\text{-}O)_2(\mu_3\text{-}OH)_{12}(H_2O)_9(O_2C\text{–})_{12}]^-$ is formed and it has a two-fold disorder with equal occupancy (Fig. S4†). In each Tb_9 cluster, nine Tb^{3+} ions are arranged in a tricapped trigonal prism (Fig. S5†): six Tb^{3+} ions are 8-coordinated with two carboxylate groups from individual $TCPE^{4-}$ ligands, four μ_3-OH, one μ_3-O, and one terminal water ligand in a distorted bicapped trigonal prismatic geometry (Fig. S6a†), while the other three coordinate to four carboxylates of four $TCPE^{4-}$ ligands, four μ_3-OH, and one apical water molecule, showing a distorted tricapped trigonal prism geometry (Fig. S6b†). From a topological viewpoint, the hexagonal prismatic Tb_9 cluster (Fig. 1b) and the rectangular $TCPE^{4-}$ ligand (Fig. 1a) serve as a 12-connected (12-c) and 4-c node to yield a (4,12)-c **shp** net (Fig. 1d). The resulting highly connected framework features a high density of aromatic rings from $TCPE^{4-}$, constituting a large π-conjugated pore surface and encompassing three types of one-dimensional (1D) channels. Among them, the largest channel A has a triangular aperture with an equilateral side length of 9.5 Å running along the *c*-axis (Fig. 1c), while the rhombus channel B and the isosceles triangular channel C are elongated along both the *a*- and *b*-axis, with the pore diameters of 7.0 and 4.5 Å, respectively (Fig. 1e and f). The total guest-accessible volume calculated using PLATON is 35.3% of the unit-cell volume, affording enough space for gas accommodation.

The phase purity of the as-synthesized sample was verified by comparing the experimental powder X-ray diffraction (PXRD) pattern to the simulation result. Immersing the

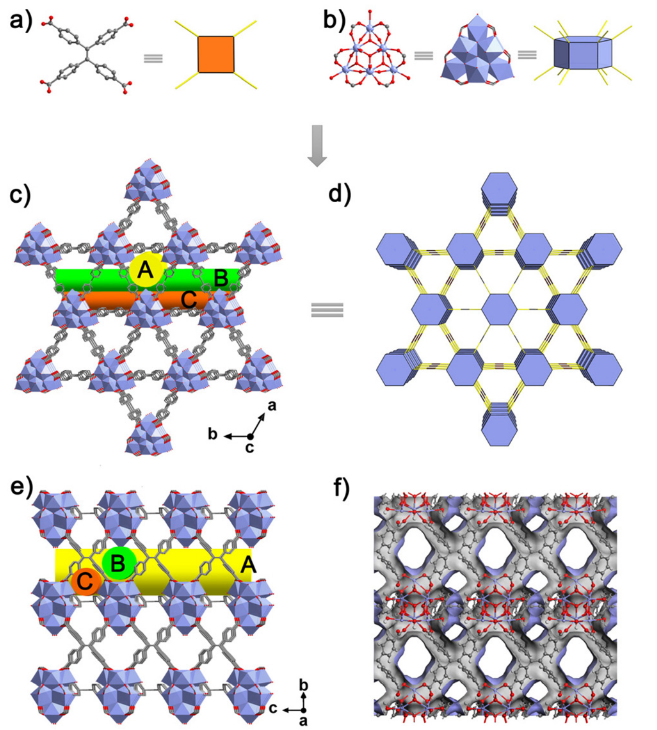

Fig. 1 (a and b) The 4-c TCPE^{4-} ligand and the 12-c nonanuclear Tb_9 cluster. (c and e) The 3D framework of **NKU-200-Tb** with three types of 1D channels along the *c*- and *a*-axis, respectively. (d) The topological simplification of the (4,12)-c **shp** net. (f) View of channels B and C in the Connolly surface.

sample in a series of organic solvents and aqueous solutions with a broad pH range of 3–12 for 24 h gave no indication of decomposition or crystallinity loss in PXRD profiles (Fig. S7 and S8†), suggesting its great chemical stability. Thermogravimetric (TG) analysis further reveals that the framework does not decompose until 500 °C (Fig. S9†), also supported by the variable-temperature (VT) PXRD data (Fig. S10†). Thus, the excellent structural stability of **NKU-200-Tb** under harsh thermal and chemical conditions places it among the most stable C_2H_6-selective MOFs reported in the literature (Table S2†), which should be attributed to not only the high connectivity of the framework, but also the strong coordination bond between the Tb^{3+} ion and carboxylate oxygen atom, according to the concept of hard and soft acids and bases (HSAB).[25] In order to investigate the permanent porosity of **NKU-200-Tb**, the sample was then subjected to methanol exchange and dynamic vacuum activation at 150 °C for 12 h. The unchanged PXRD curve confirms again the retention of its structural integrity and crystallinity after desolvation (Fig. S7†). The N_2 adsorption–desorption experiment on **NKU-200-Tb** at 77 K shows a reversible type-I isotherm (Fig. S11†), indicative of its microporous characteristic. The corresponding Brunauer–Emmett–Teller (BET) surface area and the total pore volume are then determined to be 792.7 m^2 g^{-1} and 0.32 cm^3 g^{-1} (calculated by a single point method at P/P_0 = 0.90), respectively, very close to the theoretical pore volume value of 0.35 cm^3 g^{-1} derived from single-crystal structural analysis. The estimated pore size distribution using nonlocal density functional theory lies in the range of 7–10 Å (Fig. S11†), also in agreement with the crystallographic data. The high structural stability and porosity of **NKU-200-Tb**, also proved by the N_2 adsorption curves after harsh treatments (Fig. S12†), pave the way for gas adsorptive separation.

The single-component adsorption isotherms of **NKU-200-Tb** for C_2H_6 and C_2H_4 were measured at 273 and 298 K, respectively. As shown in Fig. 2a and b, this Tb-MOF exhibits the desirable adsorption preference for C_2H_6 over C_2H_4 at both temperatures and throughout the whole pressure region, fulfilling the demand for one-step C_2H_4 purification from binary C_2H_6/C_2H_4 mixtures. At 298 K and 1 bar, the adsorption uptake of C_2H_6 on **NKU-200-Tb** reaches up to 60.27 cm^3 g^{-1} (2.69 mmol g^{-1}), much higher than that of C_2H_4 (39.95 cm^3 g^{-1}, 1.78 mmol g^{-1}) with a large uptake ratio of 151%, surpassing many leading C_2H_6-selective MOFs (Table S3†). We envisioned that the adsorption affinity order of C_2H_6 > C_2H_4 on **NKU-200-Tb** is a consequence of its nonpolar/hydrophobic pore surface. To validate the pore surface polarity, we also collected the CO_2 and water vapor adsorption isotherms at 298 K. As seen from Fig. S13,† the CO_2 uptake increases slowly and constantly over the whole pressure range and reaches 32.99 cm^3 g^{-1} (1.47 mmol g^{-1}) at 1 bar, much lower than that

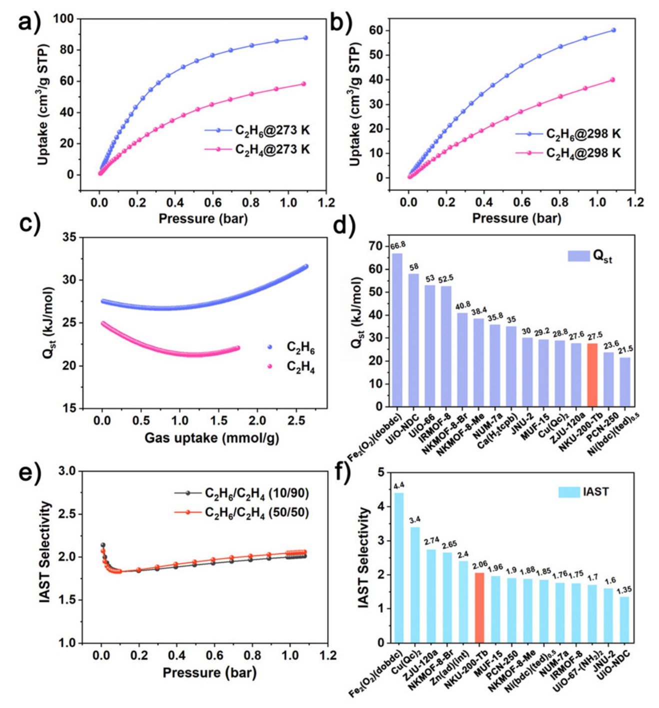

Fig. 2 (a and b) The adsorption isotherms for C_2H_6 and C_2H_4 on **NKU-200-Tb** at 273 and 298 K, respectively. (c) The coverage-dependent Q_{st} curves of C_2H_6 and C_2H_4. (d) Comparison of the zero-coverage Q_{st} of C_2H_6 with those of some representative C_2H_6-selective MOFs. (e) IAST selectivities for C_2H_6/C_2H_4 (50/50 and 10/90, v/v) mixtures at 298 K and 1 bar. (f) Comparison of the C_2H_6/C_2H_4 (50/50, v/v) selectivity at 298 K and 1 bar with those of top-performing C_2H_6-selective MOFs.

of C_2H_6, excluding the presence of open metal sites that have high affinity for CO_2.[26,27] As for water vapor, the adsorption–desorption isotherm displays a typical S-shaped curve with a hysteresis loop and an inflection point at a relatively high moisture level (Fig. S14†). This result indicates a low binding affinity toward H_2O and manifests the hydrophobicity of the inner pore surface of **NKU-200-Tb**,[16,28,29] in line with the presence of abundant aromatic rings in this system.

To quantitatively assess the binding affinities of **NKU-200-Tb** toward C_2H_6 and C_2H_4, we calculated the isosteric enthalpy of adsorption (Q_{st}) using the virial equation based on the isotherms at 273 and 298 K (Fig. S15, S16 and Table S4†). The estimated zero-coverage Q_{st} for C_2H_6 is 27.54 kJ mol^{-1}, higher than the value of 24.93 kJ mol^{-1} for C_2H_4 (Fig. 2c), thus reflecting a binding affinity order of $C_2H_6 > C_2H_4$ on **NKU-200-Tb** consistent with the inverse adsorption isotherms (Fig. 2a and b). Besides that, the coverage-dependent Q_{st} curve of C_2H_6 displays an overall ascending trend, indicative of favorable adsorbate–adsorbate interactions at higher loadings,[30,31] whereas that of C_2H_4 shows an apparent descending trend in the initial coverage range. Such an enlarged discrepancy in Q_{st} values also benefits the challenging C_2H_6/C_2H_4 separation. Noteworthily, the zero-coverage Q_{st} of C_2H_6 on **NKU-200-Tb** is significantly lower than those of many benchmark C_2H_6-selective MOFs (Fig. 2d), including NKMOF-Br/-Me (40.8/38.4 kJ mol^{-1}),[14] Fe_2O_2(dobdc) (66.8 kJ mol^{-1}),[15] IR-MOF-8 (52.5 kJ mol^{-1}),[20] and UiO-66 (53 kJ mol^{-1}).[32] The comparatively low Q_{st} value will facilitate the regeneration of **NKU-200-Tb** by avoiding harsh treatments and high energy consumption.

In order to evaluate the separation ability of **NKU-200-Tb**, we employed the ideal adsorbed solution theory (IAST) to estimate the adsorption selectivities for C_2H_6/C_2H_4 mixtures with different composition ratios. By fitting the isotherms according to the dual-site Langmuir–Freundlich equation (Fig. S17 and S18†), the C_2H_6/C_2H_4 (50/50 and 10/90, v/v) selectivities are calculated to be 2.06 and 2.01, respectively, at 298 K and 1 bar (Fig. 2e). It is worth noting that the C_2H_6/C_2H_4 (50/50, v/v) selectivity on **NKU-200-Tb** (2.06) is superior or comparable to those of most top-performing C_2H_6-selective adsorbents (Fig. 2f and Table S3†), such as PCN-250 (1.9),[33] JNU-2 (1.6),[34] Ni(bdc)(ted)$_{0.5}$ (1.85),[35] UiO-67-$(NH_2)_2$ (1.7),[36] and Zn(ad)(int) (2.4),[37] and only significantly lower than those of NKMOF-Br (2.65),[14] $Fe_2(O_2)$(dobdc) (4.4),[15] ZJU-120a (2.74),[21] and $Cu(Qc)_2$ (3.4).[22]

Such a high C_2H_6/C_2H_4 selectivity on **NKU-200-Tb** inspired us to further explore its actual separation performance. Fixed-bed dynamic breakthrough experiments were then performed at 298 K and 1 bar, with a total inlet flow rate of 10.0 mL min^{-1} by using He as the carrier gas (50%, vol%). When a C_2H_6/C_2H_4 gas mixture of an industrially relevant composition (10/90, v/v) was passed through the packed column of activated **NKU-200-Tb**, C_2H_4 was first eluted from the outlet at 314 s and quickly reached saturation, whereas the C_2H_6 impurity was still retained in the column for an additional time of 104 s, during which the C_2H_4 gas with high purity (>99.9%) can be directly harvested (Fig. 3a). The breakthrough experiments

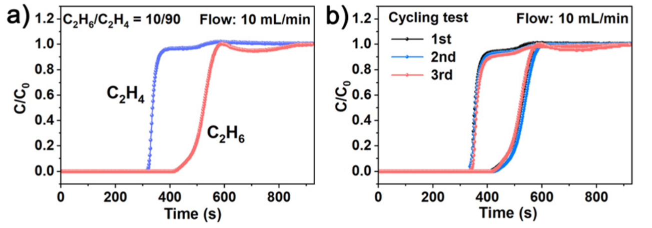

Fig. 3 (a) Dynamic breakthrough curves for a binary C_2H_6/C_2H_4 (10/90, v/v) mixture. (b) Cyclic breakthrough tests under the same conditions. All the breakthrough experiments were performed at 298 K and 1 bar, with a total flow rate of 10 mL min^{-1} using He as the carrier gas (50%, vol%).

prove that **NKU-200-Tb** is capable of separating pure C_2H_4 from a low-level of C_2H_6 through one-step adsorption without resorting to energy-intensive desorption steps. We also conducted the breakthrough experiments for an equimolar C_2H_6/C_2H_4 mixture and the results demonstrate that this MOF can also achieve one-step C_2H_4 purification from mixtures with high concentrations of C_2H_6 (Fig. S19†). For industrial applications, the stability and recyclability of an adsorbent are also important. Cyclic breakthrough tests confirm that its separation performance could be well preserved for three continuous cycles without noticeable deterioration in retention time (Fig. 3b), wherein the adsorbent was easily regenerated by heating at 150 °C under He flow for 5 h after each cycle.

To gain insight into the preferential adsorption of C_2H_6 over C_2H_4 on **NKU-200-Tb** at the molecular level, we performed DFT calculations to unveil the preferred adsorption sites and gas–framework interactions. The optimization results reveal that the most favorable trapping site for both C_2H_6 and C_2H_4 is situated at the rhombus aperture window of channel B (*i.e.*, on the pore wall of channel A) encompassed by two Tb_9 clusters and two $TCPE^{4-}$ ligands (Fig. 1e), which can be conceived of as a nanotrap (7.0 Å) possessing dense aromatic rings and suitable size for C_2H_6/C_2H_4 separation.[38] Within this confined space, the two C_2 hydrocarbon molecules adopt distinct positions and orientations (Fig. 4). With a larger vdW surface area and more C–H binding sites, C_2H_6 is grasped at the nanotrap center with an orientation perpendicular to channel B. In contrast, C_2H_4 is located close to only one side of the aperture and oriented parallel to the *a*-/*b*-axis in channel B. As a result, one C_2H_6 molecule forms seven C–H···π (3.099–3.873 Å) interactions with all four neighboring phenyl rings from two $TCPE^{4-}$ ligands, giving a static binding energy of −47.7 kJ mol^{-1} (Fig. 4a), while one C_2H_4 molecule is in contact with only one phenyl ring *via* one C–H···π (3.192 Å) bond with a lower binding energy of −36.3 kJ mol^{-1} (Fig. 4b). Clearly, the differences in the number and distance of C–H···π interactions account for the preferential adsorption of C_2H_6 over C_2H_4 and the discrepancy between the static binding energies also explains the binding affinity order of $C_2H_6 > C_2H_4$ manifested in the Q_{st}. The calculation results not only show the effectiveness of promoting the density of aromatic rings to enhance

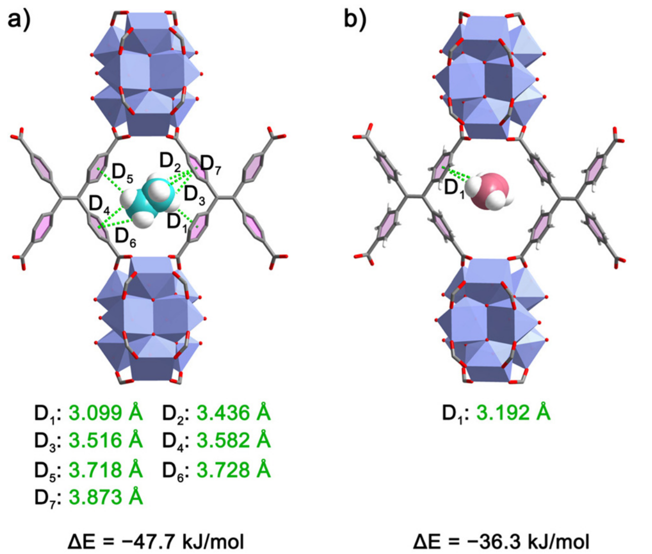

Fig. 4 (a and b) Predicted adsorption sites, interactions, and binding energies (Δ*E*) of C_2H_6 and C_2H_4 in the nanotrap of **NKU-200-Tb** obtained from the DFT optimization. The green dashed lines refer to C–H⋯π interactions.

C_2H_6 trapping and recognition ability, but also signify the synergy with pore space confinement.

In summary, a highly connected Tb-MOF (**NKU-200-Tb**) was employed to implement one-step C_2H_4 purification. Based on the reticular assembly of a nonanuclear Tb_9 cluster and the aromatic ligand $TCPE^{4-}$, the resulting MOF not only exhibits great thermal and chemical stability, but also possesses an inert/hydrophobic pore surface composed of dense nonpolar aromatic rings. As a result, **NKU-200-Tb** shows a higher adsorption capacity for C_2H_6 (60.27 $cm^3\ g^{-1}$) than for C_2H_4 (39.95 $cm^3\ g^{-1}$) at 298 K and 1 bar, highlighted with an uptake ratio of up to 151% and an excellent inverse C_2H_6/C_2H_4 selectivity of 2.06, surpassing many leading C_2H_6-selective MOFs. Further DFT calculations disclose that two Tb_9 clusters and two $TCPE^{4-}$ ligands constitute a specific size-matching nanotrap to promote the C_2H_6 adsorption by providing abundant C–H⋯π interactions within a confined pore space. With the above advantages, this MOF realizes the desirable one-step acquisition of polymer-grade C_2H_4 (>99.9%) from a binary C_2H_6/C_2H_4 (10/90, v/v) gas mixture with good recyclability, as demonstrated by breakthrough experiments. Our work not only reports a new example of one-step C_2H_4 purification adsorbents, but importantly also sheds new light on the design of paraffin-selective MOFs in terms of the engineering of inert/nonpolar pore surfaces with an enhanced confinement effect.

Author contributions

Jing-Jing Pang: investigation, visualization, data curation, and writing – original draft. Zhi-Han Ma, Qiang-Qiang Yang, Kuo Zhang, and Xin Lian: data curation. Hongliang Huang and Zhao-Quan Yao: formal analysis, conceptualization, and supervision. Baiyan Li: validation. Jian Xu: supervision, conceptualization, writing – review & editing, and funding acquisition. Xian-He Bu: resources.

Conflicts of interest

There are no conflicts to declare.

Acknowledgements

This work was supported by the National Natural Science Foundation of China (22171144 and 22001132) and the Fundamental Research Funds for the Central Universities (Nankai University). The authors would like to thank Shiyanjia Lab (**https://www.shiyanjia.com**) for the crystallographic analysis.

Notes and references

1 I. Amghizar, L. A. Vandewalle, K. M. Van Geem and G. B. Marin, New trends in olefin production, *Engineering*, 2017, **3**, 171–178.
2 J. R. Li, R. J. Kuppler and H. C. Zhou, Selective gas adsorption and separation in metal–organic frameworks, *Chem. Soc. Rev.*, 2009, **38**, 1477–1504.
3 T. Ren, M. Patel and K. Blok, Olefins from conventional and heavy feedstocks: energy use in steam cracking and alternative processes, *Energy*, 2006, **31**, 425–451.
4 D. S. Sholl and R. P. Lively, Seven chemical separations to change the world, *Nature*, 2016, **532**, 435–437.
5 W. D. Fan, X. R. Zhang, Z. X. Kang, X. P. Liu and D. F. Sun, Isoreticular chemistry within metal–organic frameworks for gas storage and separation, *Coord. Chem. Rev.*, 2021, **440**, 213968.
6 L. F. Yang, S. H. Qian, X. B. Wang, X. L. Cui, B. L. Chen and H. B. Xing, Energy-efficient separation alternatives: metal–organic frameworks and membranes for hydrocarbon separation, *Chem. Soc. Rev.*, 2020, **49**, 5359–5406.
7 H. Furukawa, K. E. Cordova, M. O'Keeffe and O. M. Yaghi, The chemistry and applications of metal–organic frameworks, *Science*, 2013, **341**, 1230444.
8 R. B. Lin, Z. J. Zhang and B. L. Chen, Achieving high performance metal–organic framework materials through pore engineering, *Acc. Chem. Res.*, 2021, **54**, 3362–3376.
9 R. B. Lin, L. B. Li, H. L. Zhou, H. Wu, C. H. He, S. Li, R. Krishna, J. P. Li, W. Zhou and B. L. Chen, Molecular sieving of ethylene from ethane using a rigid metal–organic framework, *Nat. Mater.*, 2016, **17**, 1128–1133.
10 M. Xie, Z. Lu, W. G. Lu and D. Li, Kinetic separation of C_2H_6/C_2H_4 in a cage-interconnected metal–organic framework: an interaction-screening mechanism, *Inorg. Chem. Front.*, 2022, **9**, 2697–2705.

11 B. Li, Y. Zhang, R. Krishna, K. Yao, Y. Han, Z. Wu, D. Ma, Z. Shi, T. Pham, B. Space, J. Liu, P. K. Thallapally, J. Liu, M. Chrzanowski and S. Ma, Introduction of π-complexation into porous aromatic framework for highly selective adsorption of ethylene over ethane, *J. Am. Chem. Soc.*, 2014, **136**, 8654–8660.
12 E. D. Bloch, W. L. Queen, R. Krishna, J. M. Zadrozny, C. M. Brown and J. R. Long, Hydrocarbon separations in a metal–organic framework with open iron(II) coordination sites, *Science*, 2012, **335**, 1606–1610.
13 D. F. Lv, P. J. Zhou, J. H. Xu, S. Tu, F. Xu, J. Yan, H. X. Xi, W. B. Yuan, Q. Fu, X. Chen and Q. B. Xia, Recent advances in adsorptive separation of ethane and ethylene by C_2H_6-selective MOFs and other adsorbents, *Chem. Eng. J.*, 2022, **431**, 133208.
14 S. B. Geng, E. Lin, X. Li, W. S. Liu, T. Wang, Z. F. Wang, D. Sensharma, S. Darwish, Y. H. Andaloussi, T. Pham, P. Cheng, M. J. Zaworotko, Y. Chen and Z. J. Zhang, Scalable room-temperature synthesis of highly robust ethane-selective metal–organic frameworks for efficient ethylene purification, *J. Am. Chem. Soc.*, 2021, **143**, 8654–8660.
15 L. B. Li, R. B. Lin, R. Krishna, H. Li, S. C. Xiang, H. Wu, J. P. Li, W. Zhou and B. L. Chen, Ethane/ethylene separation in a metal-organic framework with iron-peroxo sites, *Science*, 2018, **362**, 443–446.
16 S. S. Jiang, L. D. Guo, L. H. Chen, C. H. Song, B. J. Liu, Q. W. Yang, Z. G. Zhang, Y. W. Yang, Q. L. Ren and Z. B. Bao, A strongly hydrophobic ethane-selective metal–organic framework for efficient ethane/ethylene separation, *Chem. Eng. J.*, 2022, **442**, 136152.
17 W. S. Liu, S. B. Geng, N. Li, S. Wang, S. P. Jia, F. Z. Jin, T. Wang, K. A. Forrest, T. Pham, P. Cheng, Y. Chen, J. G. Ma and Z. J. Zhang, Highly robust microporous metal–organic frameworks for efficient ethylene purification under dry and humid conditions, *Angew. Chem., Int. Ed.*, 2023, **62**, e202217662.
18 S. Q. Yang and T. L. Hu, Reverse-selective metal–organic framework materials for the efficient separation and purification of light hydrocarbons, *Coord. Chem. Rev.*, 2022, **468**, 214628.
19 Z. Y. Di, C. P. Liu, J. D. Pang, S. X. Zou, Z. Y. Ji, F. L. Hu, C. Chen, D. Q. Yuan, M. C. Hong and M. Y. Wu, A metal–organic framework with nonpolar pore surfaces for the one-step acquisition of C_2H_4 from a C_2H_4 and C_2H_6 mixture, *Angew. Chem., Int. Ed.*, 2022, **61**, e202210343.
20 J. Pires, M. L. Pinto and V. K. Saini, Ethane selective IRMOF-8 and its significance in ethane–ethylene separation by adsorption, *ACS Appl. Mater. Interfaces*, 2014, **6**, 12093–12099.
21 J. Y. Pei, J. X. Wang, K. Shao, Y. Yang, Y. J. Cui, H. Wu, W. Zhou, B. Li and G. D. Qian, Engineering microporous ethane-trapping metal–organic frameworks for boosting ethane/ethylene separation, *J. Mater. Chem. A*, 2020, **8**, 3613–3620.
22 R. B. Lin, H. Wu, L. B. Li, X. L. Tang, Z. Q. Li, J. K. Gao, H. Cui, W. Zhou and B. L. Chen, Boosting ethane/ethylene separation within isoreticular ultramicroporous metal–organic frameworks, *J. Am. Chem. Soc.*, 2018, **140**, 12940–12946.
23 O. T. Qazvini, R. Babarao, Z. L. Shi, Y. B. Zhang and S. G. Telfer, A robust ethane-trapping metal–organic framework with a high capacity for ethylene purification, *J. Am. Chem. Soc.*, 2019, **141**, 5014–5020.
24 J. J. Pang, Z. Q. Yao, K. Zhang, Q. W. Li, Z. X. Fu, R. Zheng, W. Li, J. Xu and X. H. Bu, Real-time in situ volatile organic compound sensing by a dual-emissive polynuclear Ln-MOF with pronounced Ln^{III} luminescence response, *Angew. Chem., Int. Ed.*, 2023, **62**, e202217456.
25 L. Feng, K. Y. Wang, G. S. Day, M. R. Ryder and H. C. Zhou, Destruction of metal–organic frameworks: positive and negative aspects of stability and lability, *Chem. Rev.*, 2020, **120**, 13087–13133.
26 X. Ye, S. K. Xian, H. Cui, K. Tan, L. S. Gong, B. Liang, T. Pham, H. Pandey, R. Krishna, P. C. Lan, K. A. Forrest, B. Space, T. Thonhauser, J. Li and S. Q. Ma, Metal–organic framework based hydrogen-bonding nanotrap for efficient acetylene storage and separation, *J. Am. Chem. Soc.*, 2022, **144**, 1681–1689.
27 Z. Y. Di, C. P. Liu, J. D. Pang, C. Chen, F. L. Hu, D. Q. Yuan, M. Y. Wu and M. C. Hong, Cage-like porous materials with simultaneous high C_2H_2 storage and excellent C_2H_2/CO_2 separation performance, *Angew. Chem., Int. Ed.*, 2021, **60**, 10828–10832.
28 H. Furukawa, F. Gándara, Y. B. Zhang, J. C. Jiang, W. L. Queen, M. R. Hudson and O. M. Yaghi, Water adsorption in porous metal–organic frameworks and related materials, *J. Am. Chem. Soc.*, 2014, **136**, 4369–4381.
29 G. D. Wang, Y. Z. Li, W. J. Shi, L. Hou, Y. Y. Wang and Z. H. Zhu, One-step C_2H_4 purification from ternary $C_2H_6/C_2H_4/C_2H_2$ mixtures by a robust metal–organic framework with customized pore environment, *Angew. Chem., Int. Ed.*, 2022, **61**, e202205427.
30 P. Q. Liao, W. X. Zhang, J. P. Zhang and X. M. Chen, Efficient purification of ethene by an ethane-trapping metal–organic framework, *Nat. Commun.*, 2015, **6**, 8697–8705.
31 B. Y. Zhu, J. W. Cao, S. Mukherjee, T. Pham, T. Zhang, T. Wang, X. Jiang, K. A. Forrest, M. J. Zaworotko and K. J. Chen, Pore engineering for one-step ethylene purification from a three-component hydrocarbon mixture, *J. Am. Chem. Soc.*, 2021, **143**, 1485–1492.
32 J. Pires, J. Fernandes, K. Dedecker, J. R. B. Gomes, G. Pérez-Sánchez, F. Nouar, C. Serre and M. L. Pinto, Enhancement of ethane selectivity in ethane-ethylene mixtures by perfluoro groups in Zr-based metal–organic frameworks, *ACS Appl. Mater. Interfaces*, 2019, **11**, 27410–27421.
33 Y. W. Chen, Z. W. Qiao, H. X. Wu, D. F. Lv, R. F. Shi, Q. B. Xia, J. Zhou and Z. Li, An ethane-trapping MOF PCN-250 for highly selective adsorption of ethane over ethylene, *Chem. Eng. Sci.*, 2018, **175**, 110–117.

34 H. Zeng, X. J. Xie, M. Xie, Y. L. Huang, D. Luo, T. Wang, Y. F. Zhao, W. G. Lu and D. Li, Cage-interconnected metal–organic framework with tailored apertures for efficient C_2H_6/C_2H_4 separation under humid conditions, *J. Am. Chem. Soc.*, 2019, **141**, 20390–20396.
35 W. Liang, F. Xu, X. Zhou, J. Xiao, Q. Xia, Y. Li and Z. Li, Ethane selective adsorbent $Ni(bdc)(ted)_{0.5}$ with high uptake and its significance in adsorption separation of ethane and ethylene, *Chem. Eng. Sci.*, 2016, **148**, 275–281.
36 X. W. Gu, J. X. Wang, E. Y. Wu, H. Wu, W. Zhou, G. D. Qian, B. L. Chen and B. Li, Immobilization of Lewis basic sites into a stable ethane-selective MOF enabling one-step separation of ethylene from a ternary mixture, *J. Am. Chem. Soc.*, 2022, **144**, 2614–2623.
37 Q. Ding, Z. Q. Zhang, Y. L. Liu, K. G. Chai, R. Krishna and S. Zhang, One-step ethylene purification from ternary mixtures in a metal–organic framework with customized pore chemistry and shape, *Angew. Chem., Int. Ed.*, 2022, **61**, e202208134.
38 J. Q. Liu, K. Zhou, S. Ullah, J. F. Miao, H. Wang, T. Thonhauser and J. Li, Precise pore engineering of fcu-type Y-MOFs for one-step C_2H_4 purification from ternary $C_2H_6/C_2H_4/C_2H_2$ mixtures, *Small*, 2023, 2304460.